Applied Catalysis A, General 629 (2022) 118419

Contents lists available at ScienceDirect

Applied Catalysis A, General

journal homepage: www.elsevier.com/locate/apcata

Efficient nickel and copper-based catalysts supported on modified graphite materials for the hydrogen production from formic acid decomposition

B.M. Faroldi [a,b,*], J.M. Conesa [a], A. Guerrero-Ruiz [c], I. Rodríguez-Ramos [a,**]

[a] Instituto de Catálisis y Petroleoquímica (ICP-CSIC), C/Marie Curie 2, L10, Cantoblanco, 28049 Madrid, España
[b] Instituto de Investigaciones en Catálisis y Petroquímica (INCAPE-CONICET), Facultad de Ingeniería Química, Universidad Nacional Del Litoral, Santiago del Estero 2829, 3000 Santa Fe, Argentina
[c] Departamento de Química Inorgánica y Química Técnica, Facultad de Ciencias, UNED, Senda del rey, s/n, 28040 Madrid, Spain

ARTICLE INFO

Keywords:
Formic acid decomposition
nickel-based catalysts
copper based catalysts
bimetallic Ni-Cu catalysts
H2 production

ABSTRACT

Ni, Cu and Ni-Cu catalysts supported on high surface area graphite were synthesized by incipient wet impregnation. Also, the effect of doping the graphite support with alkali oxides (Li, Na and K) was studied. The catalysts were tested in the formic acid decomposition reaction to produce hydrogen. The bimetallic Ni-Cu catalyst doped with K showed the best catalytic performance with 100% conversion of formic acid at 130 °C and a 95% of selectivity to hydrogen. The turnover frequency (TOF) of the catalysts follows the order: Ni-Cu/K > NiCu/Na > Ni-Cu > Ni-Cu/Li. While the order for the apparent activation energy values is: Ni-Cu > Ni-Cu/Li > Ni-Cu/Na > Ni-Cu/K. The mechanism of the reaction is approached by programmed temperature surface reaction (TPSR) experiments and attenuated total reflectance (ATR). The greater catalytic activity of the Ni-Cu catalyst doped with potassium is ascribed to the lower stability of the formate, bicarbonate and carbonate species on its surface.

1. Introduction

Hydrogen (H_2) has significant advantages as an energy vector compared to petroleum or other conventional fossil fuels, although currently there are problems that must be solved, associated with its production, storage, and transportation [1]. Formic acid (FA) is a non-toxic renewable biomass material that can be used as an ideal liquid hydrogen carrier and achieve efficient hydrogen production. The development and utilization of FA fuel cells, using it as a hydrogen storage medium, is an effective method to solve the problem of energy depletion and environmental degradation [1,2]. However, the side reaction in the dehydration process of FA causes the catalyst to be poisoned resulting in a decrease in catalytic performance [3–5]. The development of high-performance FA dehydrogenation catalysts is of great significance for promoting the commercial application of these fuel cells.

FA is produced by chemical methods such as the hydrolysis of methyl formate, but it is also obtained in equimolar proportions together with levulinic acid, by hydrolysis of cellulose raw materials derived from biomass. Currently, with the increased interest in the production of levulinic acid and other valuable chemicals from biomass, it is important to develop processes to use the derived formic acid, since otherwise, it constitutes a waste material [1]. In this direction, the interest in the use of the decomposition reaction of FA to produce H_2 has increased remarkably. Therefore, the challenge is to produce pure H_2, with minimum CO content, at the lowest possible temperature. This demand can be achieved through the careful choice of the catalyst and the reaction conditions, which is why many research efforts are currently being devoted to this line.

The production of H_2 from FA using homogeneous and heterogeneous catalysts has been studied in aqueous [3] and vapor phases [2,3], but in most cases, formulations based on noble metals, such as Rh, Pt, Ru, Au, Ag, and Pd supported on C, Al_2O_3 and SiO_2 have been investigated [1–3]. For the vapor phase reaction, Solymosi et al. [2] found the following order of activity on a set of carbon-supported noble metals: Ir > Pt > Rh > Pd > Ru.

On the other hand, in the case of non-noble metals, molybdenum carbide has attracted great interest but it showed substantially lower activity even at high temperatures [6]. In an earlier study, we reported the catalytic performance of molybdenum carbide supported on carbon with promising results [7], though high temperatures are required for the catalyst synthesis. Moreover, the catalytic activities of supported Cu

* Corresponding author at: Instituto de Catálisis y Petroleoquímica (ICP-CSIC), C/Marie Curie 2, L10, Cantoblanco, 28049, Madrid, España.
** Corresponding author.
E-mail addresses: bfaroldi@fiq.unl.edu.ar (B.M. Faroldi), irodriguez@icp.csic.es (I. Rodríguez-Ramos).

https://doi.org/10.1016/j.apcata.2021.118419
Received 11 August 2021; Received in revised form 11 October 2021; Accepted 26 October 2021
Available online 29 October 2021

and Ni catalysts have been measured in the FA decomposition reaction, proving to be active at relatively higher temperatures (> 220 °C) than noble metal catalysts [8–10]. These authors study also the catalytic decomposition of FA on Ni, and Ni-Cu alloy powders and report an improved selectivity toward dehydrogenation reaction although lower rate when Cu is added to Ni. More recently, Pechenkin et al. described 100% conversion and 98% yield to H_2 using 10%CuO-5%CeO_2/γ-Al_2O_3 at 200 °C [11]. In this line, we have shown a Ni/SiO_2 catalyst doped with 19.3 wt% of Ca which gives 100% conversion of formic acid at 160 °C, with a 92% selectivity to hydrogen [12]. In addition, we recently reported that the bimetallic Ni-Cu system supported on carbon has better catalytic performance than the monometallic Ni or Cu catalysts [13]. Bulushev and coworkers [14] reported an improved catalytic performance for the hydrogen production from formic acid over Ni catalysts supported on carbon doped with nitrogen. These authors also suggested the Ni single atoms stabilized on the pyridinic nitrogen sites are responsible of the improved behavior of these Ni catalysts [15]. In addition, we have demonstrated that the catalytic activity and selectivity of the bimetallic Ni-Cu system is enhanced if the carbon support is doped with N-pyrrolic heteroatoms [16].

In supported Pd catalysts, the temperature required for vapor phase FA decomposition can be reduced to less than 80 °C by the addition of K_2CO_3 [1]. The difference lies in the initial stages of the reaction since FA reacts with potassium ions to give formate species dissolved in the formic acid/condensed water solution in the catalyst pores [5] increasing the overall activity of the process. In a similar way, studies of adsorption and decomposition of FA on potassium modified Cu(110) reveal that the modification of the copper surface with potassium is accompanied by a decrease in the temperatures of HCOOH decomposition [17]. In a similar way, added cesium on Cu(110) increases formate species production during FA adsorption and accelerates its decomposition [18].

Hence, in this work, the synthesis of Ni-Cu bimetallic catalysts supported on a non-porous high surface area graphite to be used in the decomposition reaction of FA in the vapor phase was carried out. The effect of doping on support with alkali metals (Li, K and Na) is studied, using in all cases an atomic ratio of alkali metal to active metal (Ni, Cu or Ni-Cu) equal to unity. The catalysts were characterized by X-ray diffraction (XRD), temperature-programmed reduction (TPR) and transmission electron microscopy (TEM). In addition, the programmed temperature surface reaction (TPSR) of FA was studied, analyzing the gases released at the outlet of the reactor employing the mass spectrometer, and attenuated total reflectance Fourier transform infrared (ATR-FTIR) spectroscopy of the used catalysts was also performed.

2. Experimental

2.1. Catalysts preparation

Nickel and copper monometallic catalysts and also bimetallic catalysts were synthesized. The technique employed to impregnate the metals was incipient wetness impregnation. Commercial high surface area graphite ($H_{400;}$ S_{BET} = 399 m^2/g) was obtained from Timcal Graphite. In all cases, the total metal concentration was 5% by weight, with 2.5% of each metal in bimetallic catalysts. The salts $Ni(NO_3)_2{\cdot}6H_2O$ (Alpha Aesar) and $Cu(NO_3)_2{\cdot}3H_2O$ (Sigma Aldrich) were used as precursors. The samples were dried at 100 °C. The following salts were used for doping with alkaline elements the graphite support: $Na_2CO_3{\cdot}H_2O$ (Alpha Aesar), KNO_3 (Panreac) and $LiNO_3$ (Sigma Aldrich). The alkaline loadings, Li (0.6% w / w), Na (2% w / w) and K (3.4% w / w) were added so that the resulting catalysts contain the same atomic charge of alkaline metal and active metal. To incorporate the dopants, the incipient wetness impregnation method was also used. These materials were dried in an oven for 12 h at 100 °C and treated in He at 500 °C for 3 h. Subsequently, the metallic charge of Ni and Cu with 2.5% of each metal, was incorporated as previously indicated.

2.2. Sample characterization

The crystalline structure of the samples was examined by X-ray diffraction (XRD) using an X´ Pert Pro PANalytical. The temperature-programmed reduction (TPR) experiments were carried out in a conventional fixed-bed flow reactor and the effluent gases were continuously monitored by a thermal conductivity detector (Konik TCD); the samples were heated up in a 5% H_2/Ar stream with a rate of 10 °C/min up to 675 °C. Transmission electron microscopy (TEM) images of the reduced catalysts were acquired using a JEOL 2100F field emission gun electron microscope equipped with an energy dispersive X-ray (EDX) detector. The fresh sample was reduced at 300 or 400 °C for 1 h in a pure H_2 stream. The catalysts were reduced ex-situ and a He flow passivation procedure was carried out at room temperature. The used samples were measured after the catalytic test and a passivation procedure to room temperature in an inert atmosphere. The samples were dispersed in ethanol and mounted on the appropriate grid for the TEM microscope. The particle size was determined by counting at least 300 particles.

2.3. Catalytic test

The catalytic activity measurements for the FA decomposition in the vapor phase were carried out in a conventional fixed-bed flow reactor. The copper and bimetallic catalysts were pretreated in H_2 flux at 300 °C for 1 h and then cooled in N_2 flux at the reaction temperature. The nickel catalyst was pretreated at 400 °C for 1 h in H_2 flux and then cooled in N_2 flux at the reaction temperature. A mixture of FA diluted with N_2 was fed to the reactor using a saturator-condenser at 15 °C (HCOOH concentration equal to 6%, with a flow of 25 ml min^{-1}). For all the experiments, 75 mg of catalyst were charged to obtain a ratio of W (weight of catalyst)/ F (total flux) equal to 5 10^{-5} g h ml^{-1}. The reactants and products were analyzed by gas chromatography (Varian 3400) fitted with a 60/80 Carboxen TM 1000 column and a thermal conductivity detector (TCD). At each temperature, a few measurements were performed in order to ensure that steady-state activity was reached. During the test, the unique products determined were CO, CO_2 and H_2. The total conversion of formic acid was determined as the sum of CO and CO_2 concentrations related to the initial concentration of FA. In addition, the CO_2 selectivity was calculated as the CO_2 concentration related to the sum of CO and CO_2 concentrations. The catalysts were studied in two heating cycles. The stability of the catalyst was evaluated over 14 h at a selected temperature. Catalytic tests with the supports proved that conversion was negligible.

2.4. Mechanism of reaction by TPSR and ATR-FTIR experiments

The temperature-programmed surface reaction (TPSR) measurements were carried out in conventional dynamic vacuum equipment coupled to a quadrupole mass spectrometer (SRS RGA-200). The catalysts were reduced before experiments in hydrogen flow at 300 or 400 °C and were degassed under high vacuum at the same temperature. The adsorption was then carried out using a 40 Torr pulse of HCOOH at 40 °C. Once the gas phase was evacuated, the desorption step was carried out at a programmed temperature, analyzing the gases released employing the mass spectrometer. The evolution of signals assigned at H_2, N_2, H_2O, CO, HCOOH, CH_2O, O_2, and CO_2 (m/e = 2, 14, 17/18, 28, 29/46, 30, 32 and 44, respectively) was followed as a function of temperature. Calibration of the relative intensity of the H_2 and CO_2 signals, m/e equal to 2 and 44, respectively, was performed. In a conventional vacuum equipment system, a certain number of moles of H_2 and CO_2 was admitted and a recirculation pump was employing for the mixture of the gases and then this stream was analyzed by the mass spectrometer.

Attenuated total reflectance Fourier transform infrared (ATR-FTIR) spectra were acquired using a Bruker Vector 22 spectrometer equipped with a germanium crystal. For the ATR experiments, the SiC was carefully separated from the solid catalyst after the catalytic tests (stability

tests for 14 h on stream) and then, was placed the sample on the crystal and collected the spectrum. A total of 256 scans with a resolution of 4 cm^{-1} were collected to measure each used catalyst.

3. Results and discussion

3.1. Catalysts characterization

Several articles have been widely investigated for CO_2 and H_2 reactions supported by noble metals (Rh, Ru, Ir, Pt and Pd) and non-noble metals (Ni, Co, Cu and Fe) [1–6,19–31]. The metal and promoters, redox properties, acid/base features and surface area of the support, the metal particle size and metal-support interactions are the key factors for obtaining a good activity/stability balance on the catalysts.

The hydrogen production from FA has been studied fundamentally on catalysts based on noble metals [1–23]. The strength of this work is to achieve high conversion and selectivity employing non-noble metals such as Ni and Cu. A graphitic material with high specific surface was used as a support and it was modified by adding alkali metals to change its surface basicity and thus favor the adsorption of HCOOH and its decomposition. The supports were modified with Na, Li and K; the percentages used were such that the number of dopant atoms is equal to the amount of active phase present in the catalyst.

The nomenclature of the catalysts only indicates the metal, Ni or Cu, in the monometallic and Ni-Cu in the bimetallic, because in all cases the support was H_{400} graphite material, and those in which an alkaline was added as /A (where A = Na, Li or K). The loadings were indicated in the experimental session.

The reducibility of the supported catalysts was studied by temperature-programmed reduction (TPR). This technique is a powerful tool for the study of the behavior of metal precursors and obtaining the strength of the oxide-support interaction. Fig. 1 shows the TPR profiles of the catalysts in the temperature range of 40–675 °C. The copper monometallic catalyst profile shows a single peak at 226 °C associated with the reduction of highly dispersed Cu^{2+} [27,32].

The nickel monometallic catalyst profile presents a reduction peak at 263 °C associated with easily reducible Ni^{2+} species and another peak at 313 °C associated with the reduction of Ni^{2+} bulk. Furthermore, a high-temperature peak, at about 416 °C, is asymmetric and wide is attributed to remaining Ni^{2+} particles and also to gasification of support carbon atoms in the vicinity of the nickel particles, which catalyze this reaction producing methane [28,33–36].

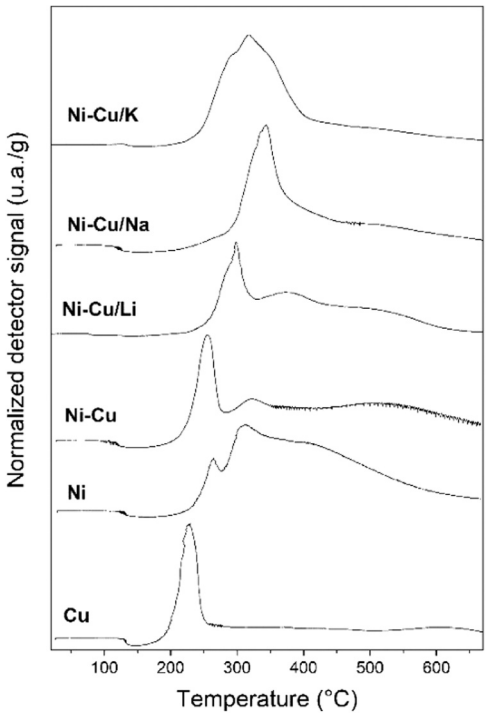

Fig. 1. Temperature-programmed reduction (TPR) profiles of the catalysts.

The profile for the bimetallic catalyst shows peaks in intermediate temperatures to the monometallic ones. The main peak is located at 254 °C, one of less intensity at 318 °C and another broad peak in the region between 400 and 600 °C with a center at 522 °C. The lower temperature peak would be associated with the reduction of Cu^{2+} and Ni^{2+} particles while the other peaks could indicate the existence of small Ni^{2+} particles which reduce at higher temperature and metal catalyzed methanation of carbon atoms around metallic particles [30,37].

On the other hand, doping with alkaline oxides slows down the reduction process of the Ni and Cu particles, causing a displacement of the TPR profiles to higher temperatures.

The catalyst doped with Li has a profile similar to the bimetallic without dopant shifted to higher temperatures. The main peak is located at 298 °C, one of less intensity at 375 °C and another broad peak in the region between 400 and 600 °C with a center at 525 °C. The catalyst doped with Na has a similar profile, too; however, a high-temperature peak less marked. The Na doped catalyst profile shifted to higher temperatures, a peak at 340, another with less intensity at 407 and the third at 506 °C completing the profile at 600 °C.

The catalyst doped with K has a different TPR profile, has a broad peak in the region between 200 and 425 °C with three positions marked at 292, 317 and 350 °C. In this catalyst, the proximity of the maximums could indicate a narrower particle sizes distribution. According to the results of the TPR experiments, it can be observed that when modifying the supports with alkali metals, the metal-support interactions were modified, displacing the reduction profiles at higher temperatures. The decrease in the reducibility of the samples which causes a shift to higher reduction temperature was observed on Ni-based catalyst doped with different contents of Na [38], on Cu catalysts modified with different metal oxides (MgO, BaO, ZnO and MnO) [39] and on Cu-Ni system doped with MnO [30].

Considering these TPR results, before the catalytic test and analysis with characterization techniques, the catalysts were pre-treated in hydrogen flow at 300 °C, except for the Ni monometallic solid, which was pre-treated in hydrogen flow at 400 °C for 1 h.

The catalysts were measured by X-ray diffraction to observe the presence of crystalline phases. The H_{400} support diffractogram (Fig. 2) exhibits the characteristic diffraction pattern of graphitic materials, with a pronounced peak at $2\theta = 26°$ due to reflection from the basal plane (002). The characteristic peaks of (100), (101), (004) and (110) crystal planes are also present [32,40].

In the diffractograms of the reduced catalysts, it is observed that there are no changes in the graphitic crystalline structure after the incorporation of the metallic phases by incipient wetness impregnation. In reduced Cu monometallic catalyst, three peaks at 43.0°, 50.5° and 74.3° assigned to the characteristic diffraction peaks of metallic copper phase (JCPDS 65-9743) [28], corresponding to (111), (200), (220) plane phase, respectively. Furthermore, a broad peak at $2\theta = 36.3°$, 42.3° (over a graphite peak) and another at approximately $2\theta = 61°$ are observed, indicative of the Cu_2O crystal structure (JCPDS 01-078-2076) probably due to the atmosphere exposure between the pretreatment and the XRD experiment. In reduced Ni monometallic catalyst, three broad peaks at 37.2°, 43.3° and 62.9° assigned to the characteristic diffraction peaks of NiO phase (JCPDS 71-1179) [41].

In the diffractogram of the reduced bimetallic Ni-Cu catalyst, no characteristic signals of Ni or Cu are detected (Fig. 2), probably due to the smaller particle sizes obtained in this solid.

When the catalysts were doped with alkali metals, three peaks at 43.0°, 50.5° and 74.3° assigned to the characteristic diffraction peaks of metallic copper corresponding to (111), (200), (220) plane phase, respectively (JCPDS 65-9743) are observed [28]. The relative intensity

of these signals concerning those of the support is greater for the catalyst with Li > K > Na. In the diffractogram of the catalyst doped with Na, signals are corresponding to sodium carbonate that remained without decomposing in the treatment at 500 °C with He flux (JCPDS 37-0451) [42]. No signals corresponding to Ni-Cu bimetallic nanoparticles were detected in the catalysts evidencing that these have sizes of 4.5 nm or less, which is the detection threshold of the XRD technique.

The distribution, shape and size of the particles were examined by transmission electronic microscopy. TEM images were taken with different magnifications of the samples reduced in H_2 at 300 °C (400 °C for the Ni monometallic catalyst). In Fig. 3, TEM images of the Cu and Ni monometallic, undoped, Na and K-doped bimetallic catalysts are shown. It can be seen that the particles of both metals are evenly distributed on the support. To estimate the mean size, 300 particles were measured, being 4.7, 4.9, 4.2, 4.3 and 5.3 nm for the Cu, Ni, Ni-Cu and Ni-Cu/Na and Ni-Cu/K catalyst, respectively. The doping with Na and K did not considerably modify the average size of the Ni-Cu bimetallic particles, but it did slightly modify the distribution of the particles (see histograms in Fig. 3).

Fig. 4 shows the images obtained for the reduced Ni-Cu/K catalyst in the STEM mode for the select area for the EDX mapping of copper (yellow), nickel (light blue), potassium (magenta) and oxygen (red). These images showed Cu particles of heterogeneous size, while Ni and K appears well dispersed. The observation of larger copper agglomerates is in agreement with the XRD results (Fig. 2). Nevertheless, the EDX analysis revealed that Ni, Cu and K particles are evenly distributed on graphitic material and coincide in occupying the same space on the support, evidencing the formation of nickel-copper particles dispersed over the K doped HSAG.

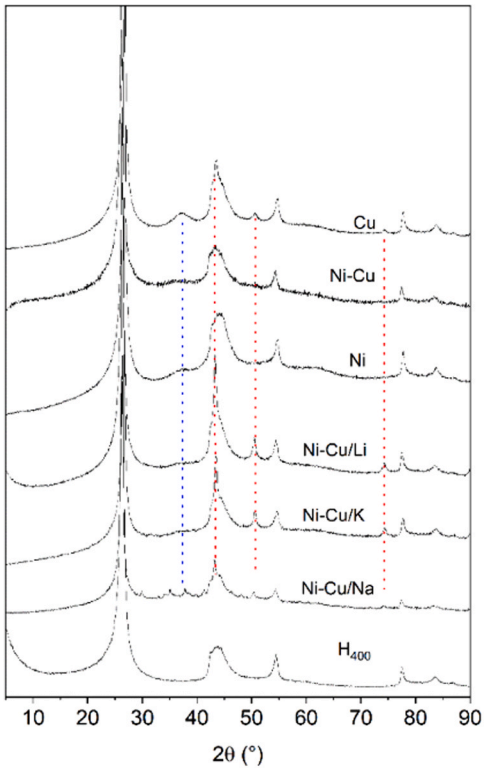

Fig. 2. X-ray diffraction (XRD) spectra of reduced Ni, Cu and Ni-Cu catalysts compared with the H_{400} support.

3.2. The catalytic performance in a fixed-bed reactor

The decomposition of formic acid is via dual-path mechanisms:

Selective dehydrogenation: $HCOOH(g) \rightarrow H_2 + CO_2 \quad \Delta G_{298} = -48.4 \quad kJ \quad mol^{-1}$

Undesirable dehydration: $HCOOH(g) \rightarrow H_2O + CO \quad \Delta G_{298} = -28.5 \quad kJ \quad mol^{-1}$

Therefore, high activity and selective catalysts are desirable for the generation of hydrogen from the decomposition of HCOOH. The catalytic activity of all catalysts was evaluated in a fix bed reactor with a mass/flow ratio (W/F) equal to 5 10^{-5} g h ml^{-1} in the temperature range of 60–200 °C to build light-off curves.

Fig. 5 shows the conversion of formic acid as a function of the reaction temperature for the series of mono and bimetallic Ni and Cu catalysts. Previous to the catalytic test, the catalysts were pre-treated in hydrogen flow at 300 °C, except for the Ni monometallic solid, which was pre-treated in hydrogen flow at 400 °C for 1 h, considering the TPR results.

It is important to note that the comparison of the catalytic activity was measured when the Ni-Cu/Na catalyst was reduced at 300 and 400 °C and no marked difference was found (Fig. S1-supplementary information). The conversion values as a function of time for the two experiments were also included, observing that they are almost coincident in the 14 h tested at 120 °C (Fig. S2-supplementary information). Therefore, it is concluded that the choice of the pretreatment temperature was adequate.

The light-off curves were performed following the same procedure in all the samples. After reducing the catalysts in H_2 flux, it was cooled in a stream of N_2 to 60 °C, and then the reaction mixture was fed with a concentration of HCOOH of 6% in N_2. After completing the curve from 0% to 100% (1st evaluation-Fig. 5), the temperature was lowered to leave it isothermal and measure the stability of the samples (Fig. 6). After 14 h on stream, the temperature was decreased and the complete light-off curve (2nd evaluation-Fig. 5) was again measured.

Table 1 compares the reaction temperature values for which the catalysts reach 50% conversion of FA. It can be seen that comparing monometallic catalysts, Ni reached the conversion value at a lower temperature (138 °C) than the Cu catalyst. However, the high selectivity to hydrogen production of the Cu catalyst is notable. Moreover, comparison with previous results obtained over a Ni/SiO_2 catalyst [13], which gives 50% conversion at 180 °C with selectivities to H_2 of 91%, demonstrates the superior performance of Ni catalyst supported on

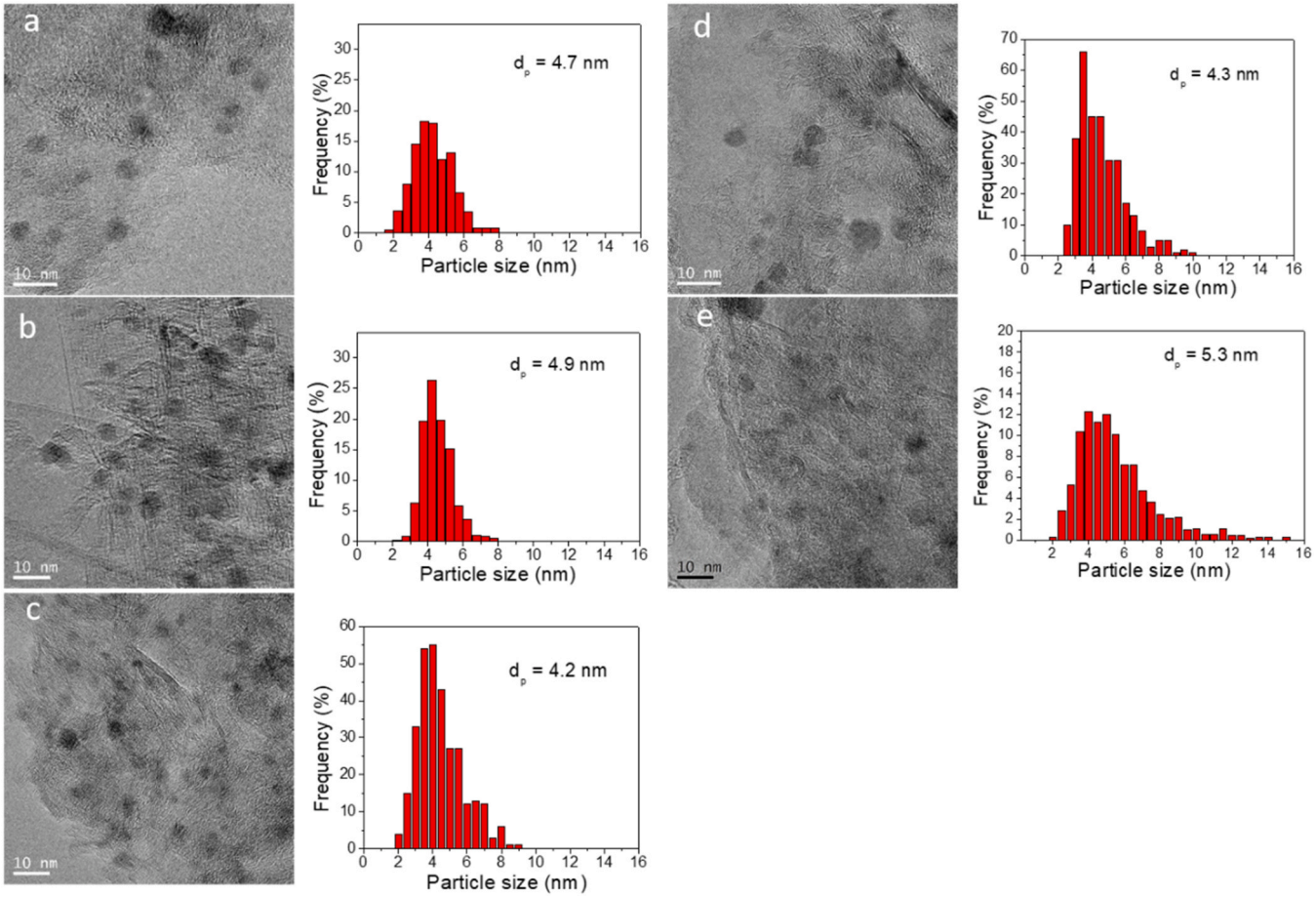

Fig. 3. Transmission electron microscopy (TEM) images of reduced samples: a) Cu, b) Ni, c) Ni-Cu, d) Ni-Cu/Na and e) Ni-Cu/K; the histograms were included.

graphite for the hydrogen production from formic acid. A composition equal to 2.5% Ni and 2.5% Cu was chosen for the bimetallic catalysts, due to the catalytic performance of the monometallic catalysts supported on HSAG-400, seeking that the solids have the highest Ni activity and at the same time the high selectivity towards H_2 provided by Cu. These results are in agreement with the DFT study of Herron et al. [43] which predicts the formation of CO_2 and H_2 on Cu(111) and Cu(100) while on Ni(111) and Ni(100) dehydration products CO and H_2O are expected. Moreover, experiments have shown the most preferable pathway for HCOOH dissociation on the stepped Ni surface was HCOOH dehydrogenation to give COOH followed by dehydroxylation to form CO [44].

In the case of the Ni-Cu bimetallic catalyst, it is observed that the activity and selectivity were intermediate, reaching 50% conversion at 145 °C, but with a selectivity of 97% towards H_2. It is worth noting the low concentration of CO (3%) in the reactor outlet stream, which is associated with a parallel dehydration reaction of HCOOH.

This work has also addressed the study of doping with alkali metals (Li, Na and K) with an atomic ratio of metal/alkaline equal to 1 to promote the basicity and the catalytic activity. Doping with K and Na shows a marked effect on the temperature at which it reaches 50% conversion of HCOOH, which in both cases was significantly lower than that of the undoped catalyst, which reveals a positive effect on the catalytic activity in these multi-component solids that make them competitive with noble metals [5]. However, the doping with Li worsened the behavior of the material, since only at the temperature of 160 °C is the 50% conversion reached, this temperature being even higher than that of the less active monometallic (Cu catalyst). Therefore, among the alkali metals studied only potassium and sodium gave promotion to the bimetallic Ni-Cu catalyst, the order of the activities measured for samples being K > Na > undoped > Li (Table 1, Fig. 5). This finding is somewhat different to that found over Pd/C catalyst for what all the alkali metal species gave promotion [1]. The doped Ni-Cu catalysts have shown high selectivity values towards hydrogen (95–97%) and the selectivities were maintained at high conversions.

The specific catalyst-mass based reaction rates obtained at 100 °C and the turnover frequency (TOF) calculated per surface metal atom are compiled in Table 2. Also, the apparent activation energies calculated from the Arrhenius plots for all the catalysts studied are given.

In Table 2 it is seen that the reaction rate and TOF value at 100 °C for the Cu catalyst are lower than (approximately half of) those obtained for the supported Ni, while the Cu-Ni bimetallic gives intermediate values. This order in catalytic activity agrees with that found in an earlier work for Ni, Cu and Ni-Cu alloy powders [10]. It is important to note that the TOF of the Ni-Cu catalyst is significantly increased when Na and specially K is added, since the TOF of the Ni-Cu is doubled for Ni-Cu/K catalyst. Thus, the TOF for the Ni-Cu/K catalyst is 0.0113 s^{-1} at 100 °C, value of reaction rate considerably higher than those reported for Ni [16] and Ni-Cu [17] supported on nitrogen doped carbon materials. However, it is very close to those reported in the literature for noble metals [1,45]. Jia et al. report a TOF value of 0.013 s^{-1} at 80 °C for a Pd/C catalyst, although this is in a great extent increased when K is added to the catalyst.

Interesting that the values of apparent activation energies for the two monometallic catalysts were similar, and also in the case of the undoped bimetallic. For catalysts modified with Li, Na and K, the apparent activation energy values were lower, the lowest value being obtained for the K-doped catalyst. It should be note that in this work the apparent activation energy values were lower than those reported in an earlier work for the decomposition of formic acid over Ni powder without support

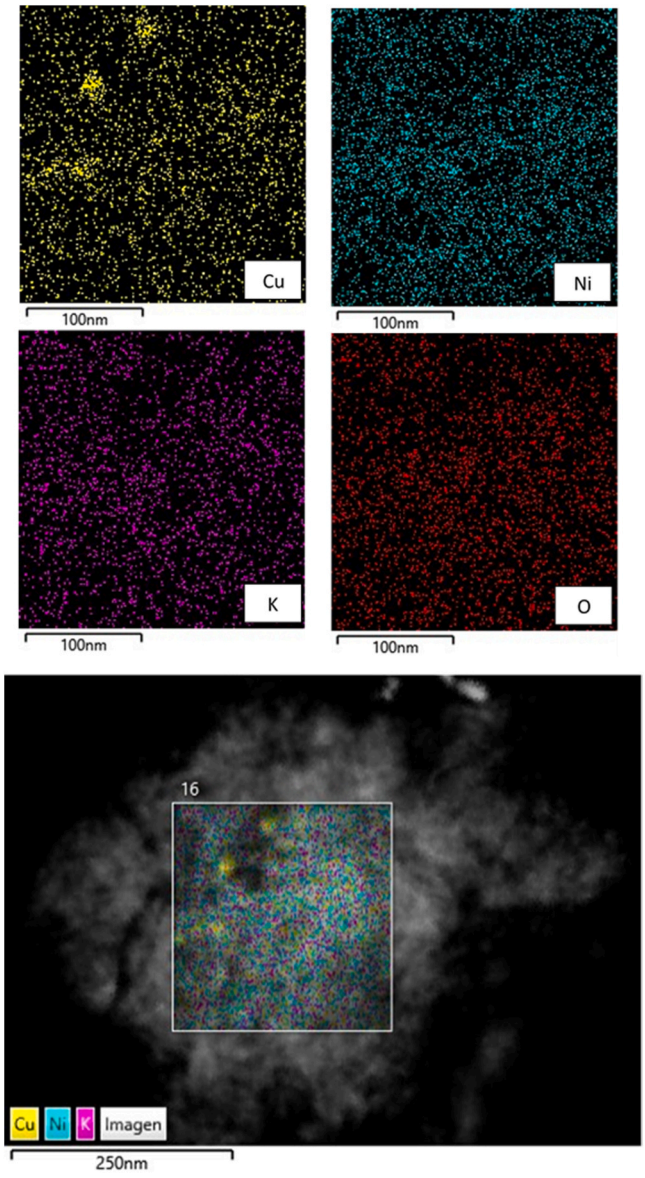

Fig. 4. Selected area for the EDX mapping for reduced Ni-Cu/K catalyst; mapping of copper (yellow), nickel (light blue), potassium (magenta) and oxygen (red).

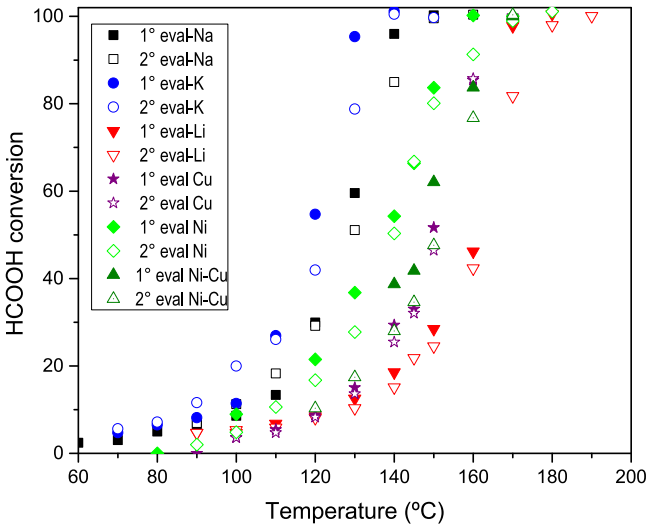

Fig. 5. The catalytic activity of Ni, Cu and Ni-Cu catalysts after reduction at 300 or 400 °C at the different reaction temperatures. HCOOH Conversions were plotted as a function of the reaction temperature (W/F = 5 10^{-5} g h ml^{-1}; feed composition: 6% $HCOOH/N_2$).

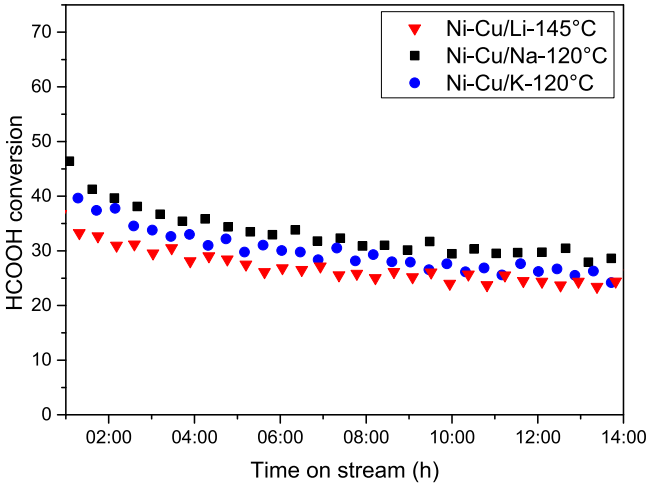

Fig. 6. Stability test of the catalysts after reduction at 300 °C in the fixed-bed reactor. (Reaction temperature = 120 or 145 °C, W/F = 5. 10^{-5} g h ml^{-1}, feed composition: 6% $HCOOH/N_2$).

and Ni catalysts supported on silica and alumina, as well as for the decomposition of Ni formate [11,46]. Also, for similar catalysts, Ni supported on carbon, the obtained values were higher in the range of 100 ± 10 kJ mol^{-1} than those calculated for the present catalysts [15, 16].

On the other hand, the catalysts were relatively stable under the conditions tested, although it can be seen in Fig. 5 that the points corresponding to the 2nd evaluation are below those obtained in the first, probably due to a restructuring of the material at the reached temperature (130–190 °C) and with conversion levels close to 100%.

In the case of catalyst doping with Li (Fig. 6) a lower activity is observed in the first hours on stream followed by a slight decay of the conversion for the temperature (145 °C) at which the stability test was carried out for this catalyst. It should be noted the marked positive effect on the conversions achieved doping the catalysts with K and Na in the whole range of temperature. The doping of K in Pd catalysts supported over SiO_2, Al_2O_3 and activated carbon has been previously reported [5]. These authors observed a significant effect of improvement in the catalytic behavior of noble metal for the formic acid decomposition. As a reaction mechanism they proposed, as a first step, the formation of a phase containing liquid formic acid condensed in the pores of the catalyst and this phase provides a reservoir for the formation of formate

Table 1
Catalytic performance of Ni, Cu and Ni-Cu samples: Temperature reaction and H_2 selectivity for 50% and 100% of HCOOH conversions (W/F = 5 10^{-5} g h ml^{-1}; feed composition: 6% $HCOOH/N_2$).

Catalysts	$T_{50\%}$	H_2 selectivity, $T_{50\%}$[a]	H_2 selectivity, $T_{100\%}$[a]	H_2/CO_2 ratio[b]
Ni	138	90	90	0.43
Cu	150	99.9	99.9	0.49
Ni-Cu	145	97	95	0.99
Ni-Cu/Li	160	93	86	1.50
Ni-Cu/Na	127	94	89	1.29
Ni-Cu/K	118	96	95	1.46

[a] H_2:CO_2 Ratio = 1.
[b] H_2/CO_2 ratio calculated by HCOOH TPD profiles.

Table 2
The catalytic performance of Ni, Cu and Ni-Cu samples: Reaction rates of HCOOH and turnover frequency (TOF) at 100 °C and apparent activation energies (Ea) (W/F = 5 10^{-5} g h ml^{-1}; feed composition: 6% HCOOH/N_2).

Catalysts	d_p (nm)	Reaction $rates_{HCOOH}$ (mol_{HCOOH} $gcat^{-1}$ h^{-1})	TOF (s^{-1})	Ea (kJ mol^{-1})
Ni	4.9	0.0042	0.0068	53.47
Cu	4.7	0.0019	0.0032	52.48
Ni-Cu	4.2	0.0038	0.0054	68.90
Ni-Cu/Li	5.0	0.0024	0.0041	40.42
Ni-Cu/Na	4.3	0.0041	0.0061	37.15
Ni-Cu/K	5.3	0.0062	0.0113	30.12

ions with the participation of K^+ ions; that later decompose to form CO_2 and H_2. In our materials, since the support is a non-porous material, condensation of formic acid is not likely to occur in pores, however, formates or oxyhydroxide phase could form in the alkali metal in the doped catalysts, these species being the reaction intermediates. In addition, the promotion effect of alkali metals increases down in the group (Li < Na < K) when the formation of these species is boosted [47].

3.3. Mechanism of reaction by TPSR and ATR experiments

Temperature programmed surface reaction (TPSR) is a powerful technique to determine the surface chemistry of bulk metal, supported metal and bulk metal oxide on supported catalysts. It can provide both qualitative and quantitative analysis of the surface active sites present on the catalyst surface, the reaction mechanisms, and kinetics occurring on the catalyst surface by using chemical probe molecules such as alcohols, carboxylates, or specific acidic-basic reacting gases. In the present paper, the experiments were carried out by adsorbing the HCOOH molecule (reactive under study) and monitoring the gas outlet flux with a mass spectrometer during desorption at programmed temperature experiments.

The TPSR experiments were carried out to understand the differences

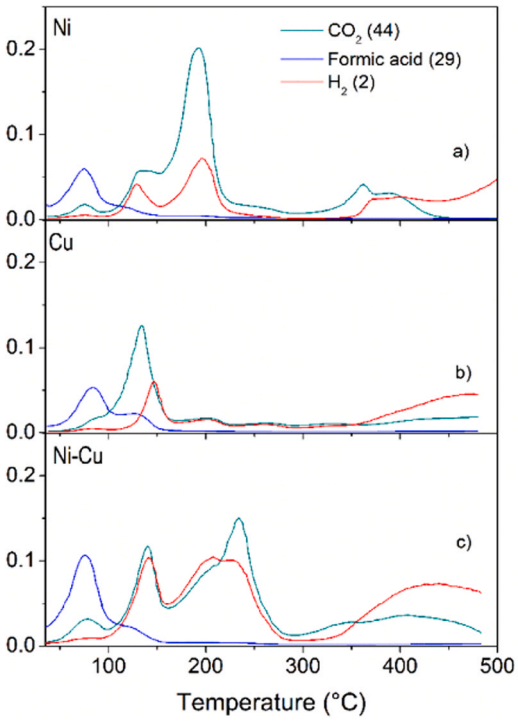

Fig. 7. Temperature programmed surface reaction profiles of Ni (a), Cu (b) and Ni-Cu (c) catalysts after 40 Torr pulse of HCOOH at 40 °C.

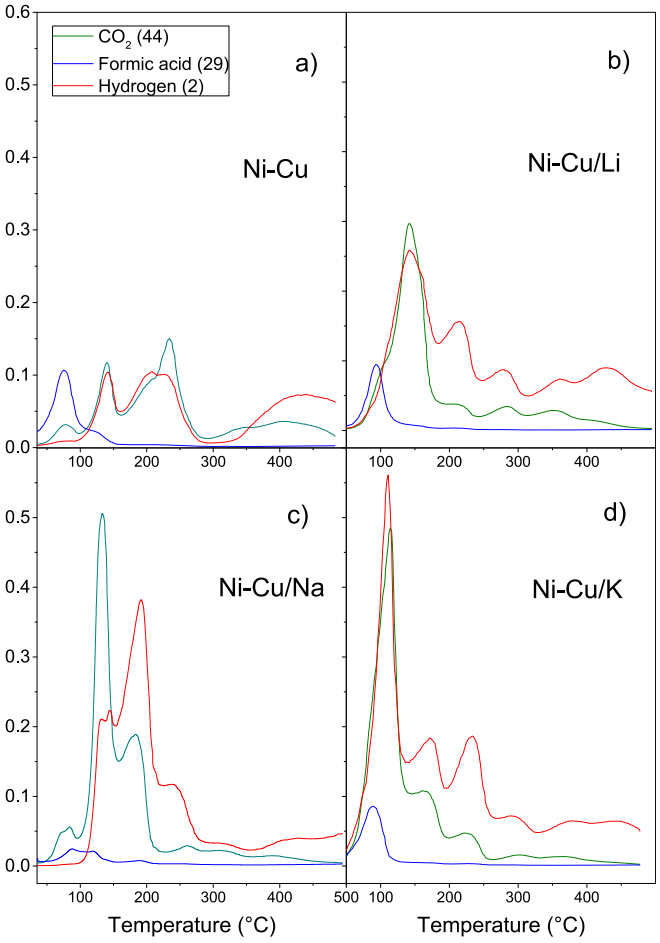

Fig. 8. Temperature programmed surface reaction profiles of Ni-Cu catalysts after 40 Torr pulse of HCOOH at 40 °C: a) Ni-Cu; b) Ni-Cu/Li; c) Ni-Cu/Na and d) Ni-Cu/K.

in the catalytic performance. The catalysts were reduced before experiments in hydrogen flow at 300 or 400 °C and were degassed in a high vacuum at the same temperature for 1 h. The adsorption was carried out using a pulse of 40 Torr of HCOOH at 40 °C. The TPSR experiments for the Ni and Cu based catalysts are shown in Figs. 7 and 8. As above stated the acid formic decomposition may proceed through either dehydrogenation giving CO_2 and H_2 and dehydration producing H_2O and CO. So, the evolution of signals assigned to H_2, N_2, H_2O, CO, HCOOH, CH_2O, O_2, and CO_2 (m/e = 2, 14, 17/18, 28, 29/46, 30, 32 and 44, respectively) was followed as a function of temperature. The evolution of the desorbed masses of H_2, CO_2 and HCOOH was plotted as a function of temperature to make the comparison clearer in Figures. The small amount of CO (m/e = 28) desorption is not plotted because the mass 28 is also secondary of CO_2 which is the major product of decomposition and the determination of real CO production is prone to considerable error.

The TPSR experiments for the Ni, Cu and Ni-Cu catalysts are shown in Fig. 7. At lower temperatures (< 100 °C) the desorption of the unreacted HCOOH is observed and above 50 °C the decomposition process begins to produce H_2 and CO_2. This behavior was similar for the three samples compared in this figure.

For the Ni catalyst, in Fig. 7a the H_2 and CO_2 profiles show in addition to the 80 °C peak a maximum at 125 °C, then an increase mainly in CO_2 signal with another maximum at 200 °C. After that, both signals remain at zero until the region of 300–400 °C where the decomposition of the fraction of retained FA in the catalyst occurs. Previous studies using spectroscopic techniques and temperature

programmed desorption (TPD) of FA adsorption over Ni(111) surfaces [48] reported the formation of bidentate formates at low temperature which transformed to monodentate formates and decomposed in the 25–225 °C temperature range, producing CO_2 at 100 °C and also CO at 157 °C.

For the Cu catalyst, Fig. 7b, the HCOOH signal had two steps marked of desorption at 80 and 140 °C. In addition, at that temperature of 140 °C, a maximum of CO_2 production is observed and also in the H_2 signal at 150 °C. The adsorption and decomposition of formic acid on clean Cu(110) has been previously studied by means of thermal desorption mass spectroscopy [14,49]. On the Cu(110) surface the formate species formed is stable up to 127 °C, but decomposes to simultaneously evolve H_2 and CO_2 in TDS peaks at 190–200 °C. However, the temperature for HCOOH decomposition on Cu metallic powder has been shown to be lower than on Cu(110) surface [50]. In addition, the reaction is structure sensitive on Cu catalysts since Cu(100) and Cu (211) bind HCOO much more strongly than Cu(111) and have varied barriers for the likely rate determining step, formate species dehydrogenation [51].

For the bimetallic catalyst, Fig. 7c, the H_2 and CO_2 profiles are not the results of adding the profiles obtained for the monometallic catalysts. The low-temperature region is similar to that mentioned for monometallics, however, the CO_2 and H_2 signals show a maximum at 145 °C and another increase in the region of 160 and 250 °C. For this catalyst, a remarkable coincidence is observed in the profiles of both gaseous products.

In Fig. 8, the undoped bimetallic catalyst and the catalysts doped with K, Li and Na are compared. The objective of adding an alkali metal to the Ni-Cu bimetallic catalyst was to promote the catalytic activity by increasing its basicity. These alkali metals could also favor the formation of stable carbonates at high temperatures [14].

In the three cases, the alkali/active metal ratio was maintained to compare the effect caused by each one. It is possible to observe that the profiles have similar shapes although with different relative intensities (Fig. 8b–d). In addition, for all the catalysts was observed that at a lower temperature (< 120 °C) desorption of the unreacted HCOOH is observed and above 50 °C the decomposition process begins to produce H_2 and CO_2. Relative to the non-alkali modified Ni-Cu catalyst the intensity of the CO_2 and H_2 profiles for the alkali modified catalysts have considerably increased which is related with the promotion by the alkali of the formate species formation [13].

The potassium-doped catalyst shows a first maximum of the product signals at 105 °C, this being the lowest temperature observed for all the catalysts under study. This could explain the higher activity observed for this catalyst.

The sodium-doped catalyst shows the first maximum at 135 °C where a greater intensity of the CO_2 signal and retention of H_2 at that temperature was observed. This behavior could be related to the sodium precursor salt (sodium carbonate) employed in this solid.

The lithium-doped catalyst shows a first signal at 145 °C of both products. It can be seen, that the Ni and Cu monometallic, undoped bimetallic and Li-doped catalysts had lower adsorption of HCOOH and subsequent lower production of H_2 and CO_2 (Figs. 7a–c and 8b). This could be related to the lower catalytic activity observed for these catalysts.

The H_2/CO_2 ratio was determined from the HCOOH TPD profiles (Table 1) using a calibration of the relative intensity of the H_2 and CO_2 signals, m/e equal to 2 and 44, respectively. The monometallic catalysts present values of the H_2/CO_2 intensity ratio less than 1 (0.43 and 0.49), this could indicate that the fraction of hydrogen not released after decomposition is retained, forming hydride or formate species. For the bimetallic non-doped catalyst, a desorbed equimolecular ratio is observed, indicating that neither H_2 nor CO_2 are retained on the catalyst. The catalysts doped with K, Na and Li present values of H_2/CO_2 ratios greater than 1, indicating stronger adsorption of CO_2, probably forming carbonate species [14]. If the samples doped with Na and K are compared, it can be seen that in the first one, a greater amount of CO_2 ($H_2/CO_2 = 0.5$) was desorbed by the decomposition of formic acid at a lower temperature (100–150 °C range, Fig. 8c). For the other catalyst, Ni-Cu/K, the production of H_2 and CO_2 was equimolar as corresponds to the formic acid decomposition reaction at a lower temperature (100–150 °C range, Fig. 8d). The sample doped with Na presents greater desorption of H_2 at a higher temperature. This indicates in the case of Na greater stability of species, for example, formate or bicarbonate type, that store hydrogen in this solid. The presence of formate, bicarbonate and carbonate species in the catalysts used on reaction was confirmed by attenuated total reflectance (ATR) (Fig. 9).

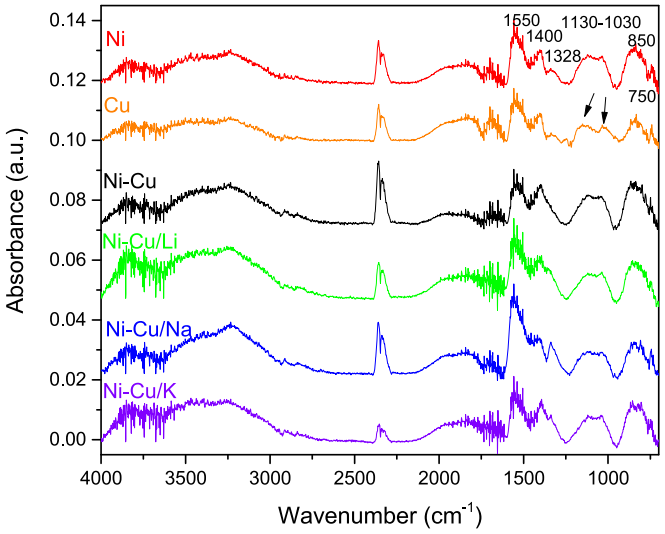

Fig. 9. Attenuated total reflectance (ATR) spectra of used catalysts (after the stability tests for 14 h on stream).

The spectra of the used catalysts show signals assigned to bridged carbonates ($\nu_{(C\overline{\quad}O)}$: 1730–1640 cm^{-1}; $\nu_{as(COO)}$: 1285–1280 cm^{-1}; $\nu_{s(COO)}$: 1020–1000 cm^{-1}), bidentate carbonates ($\nu_{(C\overline{\quad}O)}$: 1670–1530 cm^{-1}; $\nu_{as(COO)}$: 1270–1220 cm^{-1}; $\nu_{s(COO)}$: 1030–980 cm^{-1}), monodentate carbonates ($\nu_{as}(CO_3^{2-})$: 1530–1470 cm^{-1}; $\nu_s(CO_3^{2-})$: 1370–1300 cm^{-1}; $\nu_{(C\text{-}O)}$: 1080–1040 cm^{-1}), carbonites ($\nu_{as(CO2)}$: 1495–1478 cm^{-1}; $\nu_{s(CO2)}$: 890–717 cm^{-1}) and formates species ($\nu_{as(COO\text{-})}$: 1605–1540 cm^{-1}; $\nu_{s(COO\text{-})}$: 1370–1345 cm^{-1}) [44,52–54]. It is important to note that the signals associated with the formate species present a higher relative intensity for the Na-doped catalyst, being consistent with what was observed in the formic acid TPSR experiments. Probably the lower stability of these species in the catalyst doped with potassium is the factor that determines their greater capacity to promote the catalytic activity.

4. Conclusions

The synthesis of Ni-Cu bimetallic catalysts supported on a non-porous high surface area graphite was performed. The catalysts were employed in the decomposition reaction of formic acid in the vapor phase. The effect of doping on support with alkali metals (Li, K and Na) was studied, using in all cases an atomic ratio of alkali metal to active metal (Ni, Cu or Ni-Cu) equal to unity.

The bimetallic Ni-Cu catalyst has an intermediate behavior of monometallic, with high catalytic activity for the decomposition of formic acid and high selectivity for the production of hydrogen (97%). The comparative study of the promotion of the Ni-Cu catalyst with the alkali metals Li, Na and K shows that the catalyst doped with K has the best behavior in the formic acid decomposition reaction. TPRS experiments show that formate, bicarbonate or carbonate species decompose at different temperatures depending on the alkali metal present in the catalyst and the formation/decomposition of these species turns out to be an important factor in promoting catalytic activity. The sample doped

with Na presents greater desorption of H_2 at a higher temperature and a higher relative intensity of the formate species was observed in the used catalyst by ATR. The potassium-doped catalyst shows the maximum production of H_2 and CO_2 equimolar at 105 °C, being the lowest temperature observed for all the catalysts under study. This could explain the higher activity observed for this catalyst.

The bimetallic catalyst doped with K showed 100% conversion of formic acid at 130 °C with a 95% of selectivity to hydrogen. Also, all the tested materials were promising for their application since they showed catalytic behaviors close to those of noble metals reported in the literature.

CRediT authorship contribution statement

B.M. Faroldi: Conceived and designed the experiments, Investigation, Writing – original draft. **J.M. Conesa:** Investigation, collaborated with the catalytic and TPRS experiments. **A. Guerrero-Ruiz**: Writing – review & editing. **I. Rodríguez-Ramos:** conceived and designed the experiments, Project administration, Writing – review & editing, Funding acquisition, B.F. and I.R.R. conceived and designed the experiments. All authors discussed the results and contributed to the manuscript.

Declaration of Competing Interest

The authors declare that they have no known competing financial interests or personal relationships that could have appeared to influence the work reported in this paper.

Acknowledgments

The authors wish to acknowledge the financial support received from the Spanish Agencia Estatal de Investigación (AEI) and EU (FEDER) (projects CTQ2017-89443-C3-1-R, CTQ2017-89443-C3-3-R, PID2020-119160RB-C21 and PID2020-119160RB-C22). B. Faroldi thanks CONICET for Postdoctoral External Fellowship Program.

Appendix A. Supplementary information

Supplementary data associated with this article can be found in the online version at doi:10.1016/j.apcata.2021.118419.

References

[1] L. Jia, D.A. Bulusheva, S. Beloshapkin, J.R.H. Ross, Appl. Catal. B 160–161 (2014) 35–43.
[2] F. Solymosi, Á. Koós, N. Liliom, I. Ugrai, J. Catal. 279 (2011) 213–219.
[3] Z.L. Wang, J.M. Yan, H.L. Wang, Y. Ping, Q. Jiang, Sci. Rep. 2 (2012) 598–603.
[4] L. Jia, D.A. Bulushev, J.R.H. Ross, Catal. Today 259 (2016) 453–459.
[5] P. Ferreira-Aparicio, I. Rodriguez-Ramos, J.A. Anderson, A. Guerrero-Ruiz, Appl. Catal. A 202 (2000) 183–196.
[6] D.W. Flaherty, S.P. Berglund, C.B. Mullins, J. Catal. 269 (2010) 33–43.
[7] D.H. Carrales-Alvarado, A.B. Dongil, J.M. Fernández-Morales, M. Fernández-García, A. Guerrero-Ruiz, I. Rodríguez-Ramos, Catal. Sci. Technol. 10 (2020) 6790–6799.
[8] E. Iglesia, M. Boudart, J. Catal. 81 (1983) 204–213.
[9] E. Iglesia, M. Boudart, J. Catal. 81 (1983) 214–223.
[10] E. Iglesia, M. Boudart, J. Catal. 81 (1983) 224–238.
[11] A. Pechenkin, S. Badmaev, V. Belyaev, V. Sobyanin, Energies 12 (18) (2019) 3577–3586.
[12] B. Faroldi, M.A. Paviotti, M. Camino-Manjarrés, S. González-Carrazán, C. López-Olmos, I. Rodríguez-Ramos, Nanomaterials 9 (2019) 1516.
[13] B.M. Faroldi, J.M. Conesa, A. Guerrero Ruiz, I. Rodríguez Ramos, in: Proceedings of the X.X.I. Congreso Argentino de Catálisis y X Congreso de Catálisis del Mercosur, Santa Fe, Argentina, September 2019, pp. 216–222.
[14] A.D. Nishchakova, D.A. Bulushev, O.A. Stonkus, I.P. Asanov, A.V. Ishchenko, A. V. Okotrub, L.G. Bulusheva, Energies 12 (2019) 4111–4121.
[15] D.A. Bulushev, A.D. Nishchakova, S.V. Trubina, O.A. Stonkus, I.P. Asanov, A. V. Okotrub, L.G. Bulusheva, J. Catal. 402 (2021) 264–274.
[16] D.H. Carrales-Alvarado, C. López-Olmos, A.B. Dongil, A. Kubacka, A. Guerrero-Ruiz, I. Rodríguez-Ramos, Appl. Catal. B. 298 (2021) 120604.
[17] P.M. Moller, P.J. Godowski, J. Onsgaard, Vacuum 54 (1999) 31–36.
[18] F.C. Henn, J.A. Rodriguez, C.T. Campbell, Surf. Sci. 236 (1990) 282–312.
[19] K. Nagaoka, M. Okamura, K. Aika, Catal. Commun. 2 (2001) 255–260.
[20] F. Mark, W. Maier, J. Catal. 164 (1996) 122–130.
[21] U.L. Portugal, C.M. Marques, E.C. Araujo, E.V. Morales, M.V. Giotto, J.M.C. Bueno, Appl. Catal. A 193 (2000) 173–183.
[22] M. Bradford, M.A. Vannice, J. Catal. 183 (1999) 69–75.
[23] J. Wei, E. Iglesia, J. Phys. Chem. B 108 (2004) 7253–7262.
[24] J.F. Munera, S. Irusta, L.M. Cornaglia, E.A. Lombardo, D.V. Cesar, M. Schmal, J. Catal. 245 (2007) 25–34.
[25] A.M. O'Connor, Y. Schuurman, J.R.H. Ross, C. Mirodatos, Catal. Today 115 (2006) 191–198.
[26] D. Pakhare, J. Spivey, Chem. Soc. Rev. 43 (2014) 7813–7837.
[27] Y. Cui, H. Zhang, H. Xu, W. Li, Appl. Catal. A 318 (2007) 79–88.
[28] C.E. Daza, J. Gallego, J.A. Moreno, F. Mondragon, S. Moreno, R. Molina, Catal. Today 133 (2008) 357–366.
[29] M. Usman, W.M.A. Wan Daud, H.F. Abbas, Renew. Sustain. Energy Rev. 45 (2015) 710–744.
[30] D.A.J.M. Ligthart, R.A. van Santen, E.J.M. Hensen, J. Catal. 280 (2011) 206–220.
[31] R. Arvaneh, A. Azizzadeh Fard, A. Bazyari, S. Mehdi Alavi, F. Jokar Abnavi, Korean J. Chem. Eng. 36 (2019) 1033–1041.
[32] L. Wang, N. Zuo, Q. Liu, D. Xie, M. Sun, N. Mominou, Y. Ma, C. Jing, J. Alloy. Compd. 855 (2021) 157516–157525.
[33] J. Gao, Z. Hou, J. Guo, Y. Zhu, X. Zheng, Catal. Today 131 (2008) 278–284.
[34] C. López-Olmos, A. Guerrero-Ruiz, I. Rodríguez-Ramos, Catal. Today 357 (2020) 132–142.
[35] A.B. Dongil, B. Bachiller-Baeza, I. Rodríguez-Ramos, J.L.G. Fierro, N. Escalona, RSC Adv. 6 (2016) 26658–26667.
[36] M.V. Morales, J.M. Conesa, A. Guerrero-Ruiz, I. Rodríguez-Ramos, Carbon 182 (2021) 265–275.
[37] T.A. Le, M.S. Kim, S.H. Lee, T.W. Kim, E.D. Park, Catal. Today 293–294 (2017) 89–96.
[38] N. Li, Z. Li, N. Wang, J. Yu, Y. Yang, ACS Omega 6 (3) (2021) 2346–2353.
[39] C. López-Olmos, M.V. Morales, A. Guerrero-Ruiz, I. Rodríguez-Ramos, Ind. Eng. Chem. Res. 59 (2020) 16626–16636.
[40] W. Han, H. Yan, H. Tang, Y. Li, H. Liu, React. Kinet. Mech. Catal. 113 (2014) 361–374.
[41] M.A. Paviotti, B.M. Faroldi, L.M. Cornaglia, J. Environ. Chem. Eng. 9 (2021) 105173–105186.
[42] S. Medina-Carrasco, J.M. Valverde, Cryst. Growth Des. 18 (2018) 4578–4592.
[43] J.A. Herron, J. Scaranto, P. Ferrin, S. Li, M. Mavrikakis, ACS Catal. 4 (2014) 4434–4445.
[44] X. Li, K. Xuan, Y. Zhu, G. Chen, G. Yang, Appl. Surf. Sci. 452 (2018) 87–95.
[45] O. Podyacheva, A. Lisitsyn, L. Kibis, A. Boronin, O. Stonkus, V. Zaikovskii, A. Suboch, V. Sobolev, V. Parmon, Energies 12 (2019) 3976.
[46] E. Iglesia, M. Boudart, J. Catal. 81 (1983) 325–332.
[47] J. Ding, C. Yu, J. Lu, X. Wei, W. Wang, G. Pan, Appl. Energy 263 (2020), 114681.
[48] C. Hirose, A. Bandara, J. Kubota, A. Wada, K. Domen, Appl. Phys. B 68 (1999) 559–565.
[49] Y. Yao, F. Zaera, Surf. Sci. 646 (2016) 37–44.
[50] Y. Tang, C.A. Roberts, R.T. Perkins, I.E. Wachs, Surf. Sci. 650 (2016) 103–110.
[51] S. Li, J. Scaranto, M. Mavrikakis, Top. Catal. 59 (2016) 1580–1588.
[52] B.W.J. Chen, M. Mavrikakis, ACS Catal. 10 (2020) 10812–10825.
[53] J. Kubota, A. Bandara, A. Wada, K. Domen, C. Hirose, Surf. Sci. 368 (1996) 361–365.
[54 K. Hadjiivanov, G. Vayssilov, Adv. Catal. 47 (2002) 307–511.